■ Coordination Chemistry

# Non-Oxido-Vanadium(IV) Metalloradical Complexes with Bidentate 1,2-Dithienylethene Ligands: Observation of Reversible Cyclization of the Ligand Scaffold in Solution

Dirk Schlüter,[a] Florian Kleemiss,[a, e] Malte Fugel,[a] Enno Lork,[a] Kunihisa Sugimoto,[b, d] Simon Grabowsky,[a, e] Jeffrey R. Harmer,[c] and Matthias Vogt*[a]

**Abstract:** Derivatives of 1,2-dithienylethene (DTE) have superb photochromic properties due to an efficient reversible photocyclization reaction of their hexatriene structure and, thus, have application potential in materials for optoelectronics and (multi-responsive) molecular switches. Transition-metal complexes bearing switchable DTE motifs commonly incorporate their coordination site rather distant from the hexatriene system. In this work the redox active ligand 1,2-bis(2,5-dimethylthiophen-3-yl)ethane-1,2-dione is described, which reacts with [V(TMEDA)$_2$Cl$_2$] to give a rare non-oxido vanadium(IV) species **3(M,M/P,P)**. This blue complex has two bidentate en-diolato ligands which chelate the V$^{IV}$ center and give rise to two five-membered metallacycles with the adjacent hexatriene DTE backbone bearing axial chirality. Upon irradiation with UVA light or prolonged heating in solution, the blue compound **3(M,M/P,P)** converts into the purple atropisomer **4(para,M/para,P)**. Both complexes were isolated and structurally characterized by single-crystal X-ray diffraction analysis (using lab source and synchrotron radiation). The antiparallel configuration (M or P helicity) present in both **3(M,M/P,P)** and **4(para,M/para,P)** is a prerequisite for (reversible) 6$\pi$ cyclization reactions. A CW EPR spectroscopic study reveals the metalloradical character for **3(M,M/P,P)** and **4(para,M/para,P)** and indicates dynamic reversible cyclization of the DTE backbone in complex **3(M,M/P,P)** at ambient temperature in solution.

## Introduction

Oxido-vanadium compounds, mostly in the oxidation state +V and +VI, are intensively studied for applications in a diverse range of areas. For instance, vanadate and vanadyl derivatives possess significant importance as biologically active species,[1, 2] have been shown to possess insulin-mimetic properties[3–6] and are important catalytic species in various oxidation reactions.[7–9] In contrast, non-oxido vanadium(IV) compounds are less frequently reported in the literature. Sproules, Wieghardt and co-workers described V$^{IV}$ complexes with non-innocent ligand-sets.[10] A prominent compound is amavadin, which is a naturally occurring example of a non-oxido V$^{IV}$ coordination complex,[11] which was initially isolated from the toadstool *Amanita muscaria*.[12] Vanadocene dichloride and derivatives thereof have been investigated with respect to their antitumor activity.[13] Vanadium coordination compounds show a broad range of potential applications in medicinal chemistry including the treatment of endemic tropical and various heart muscle diseases. A concise overview was recently given by Rehder.[9]

Herein, we characterize a class of non-oxido vanadium(IV) complexes bearing two chelating en-diolato ligands with a 1,2 dithienylethene (DTE) motif as backbone, Scheme 1 **F**, **G**. DTE motifs have received considerable attention due to their superior photochromic properties, that is, DTEs undergo reversible photocyclization reactions with an associated characteristic color change. They have a significant application potential as a new photoswitchable material for optoelectronics and (multiresponsive) molecular switches. The photochromic properties of DTEs are characterized, for instance, by a high fatigue resistance, high quantum yields, the robust thermal stability of

[a] D. Schlüter, F. Kleemiss, Dr. M. Fugel, Dr. E. Lork, PD Dr. S. Grabowsky, Dr. M. Vogt
Institut für Anorganische Chemie und Kristallographie
Universität Bremen, Leobener Str. 3 and 7, 28359 Bremen (Germany)
E-mail: mavogt@uni-bremen.de

[b] Prof. Dr. K. Sugimoto
SPring-8/JASRI, 1-1-1 Kouto, Sayo-cho, Sayo-gun, Hyogo 679-5198 (Japan)

[c] Prof. Dr. J. R. Harmer
Center of Advanced Imaging (CAI), University of Queensland
St. Lucia, QL (Australia)

[d] Prof. Dr. K. Sugimoto
Institute for Integrated Cell-Material Sciences (iCeMS), Kyoto University
Yoshida-Ushinomiya-cho, Sakyo-ku, Kyoto 606-8501 (Japan)

[e] F. Kleemiss, PD Dr. S. Grabowsky
Current address: Abteilung für Chemie und Biochemie
Universität Bern, Freiestrasse 3, 3012 Bern (Switzerland)
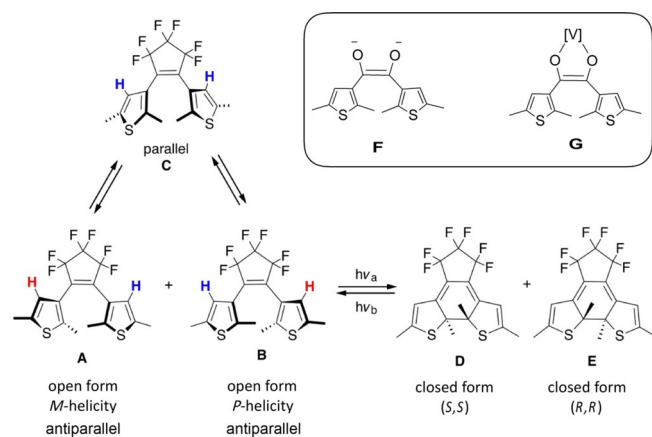
**Scheme 1.** Atropisomers and photocyclization of 1,2-bis(2,5-dimethyl-3-thienyl)perfluorocyclopentane.

all isomers, and a rapid response to the external stimulus. They are also responsive in the solid state.[14–17] DTEs have been discussed as functional key components in a range of applications including conductive polymers,[18] multiresponsive molecular switches,[19] optical memory devices,[20] photoresponsive building blocks that can regulate supramolecular architectures,[21,22] a selective fluorescent probe for the detection of metal ions,[23] and photoresponsive self-assemblies at liquid–solid interfaces.[24] DTE derivatives that show turn-on mode fluorescence are promising candidates for applications in super-resolution fluorescence microscopy[24] and all-optical transistors.[26] A current active field of research addresses the control of motion in covalently bonded molecular systems, which is closely associated with the design of "molecular machines". In this aspect, the control of conformational change is crucial. For instance, an established approach is the control of conformational change about a single bond triggered by an external stimulus.[27] Against this background, DTEs are reported to possess axial chirality resulting in the formation of atropisomers. Atropisomers (from Greek *atropos* = not turning) are stereoisomers (rotamers) occurring due to a hindered rotation about a single bond. Their rotational interconversion is hampered by a large-enough barrier to allow the individual "minus" ($M$ or $R_a$) and "plus" ($P$ or $S_a$) atropisomers to be "locked" (see Scheme 1 **A**, **B**, ).[28] Oki defines atropisomers and distinguishes them from rotamers on the basis that they are fully resolvable at ambient temperature, corresponding to a barrier of interconversion of $> 23.3$ kcal mol$^{-1}$.[29] Atropisomerism, especially in biaryl derivatives bearing a chiral axis between two aromatic moieties, has been intensively exploited for the design of chiral ligand systems that find numerous applications in the field of asymmetric catalysis.[30–35] Atropisomeric chirality, not only restricted to biarylic systems, is important in medicinal chemistry,[36] has pharmaceutical implications as an alternative source for the production of chiral drugs,[37] and can be found in a variety of natural products.[28,38]

1,2-Bis(2,5-dimethyl-3-thienyl)perfluorocyclopentane, a typical example for a photochromic DTE-based derivative with axial chirality, is shown in Scheme 1 **A–E**.[15,16] The compound

forms the open-ring isomer with parallel aligned thienyl groups (**C**) and the respective enantiomeric antiparallel forms with $M$ (**A**) and $P$ helicity (**B**).[21,39] The photoinduced cyclization reaction can only occur from the antiparallel conformers **A** and **B** and gives rise to the closed enantiomeric forms **D** and **E** with ($S,S$) and ($R,R$) configurations,[21] respectively, based on the asymmetric carbon atoms in 2-position of the thiophene units (see Scheme 1).[39] It must be noted that the parallel atropisomer cannot directly undergo photochemical cyclization,[40] and its coexistence with the antiparallel isomers lowers the efficiency of the switching process. Consequently, effort has been spent to increase the relative amount of the antiparallel atropisomers **A** and **B**.[41]

With this background, we now report on the DTE-based bidentate ligand (**F**) equipped with an en-diolato motif. Chelation of a vanadium(IV) metal center gives rise to the formation of a five-membered metallacycle (**G**). These non-oxido vanadium(IV) atropisomeric complexes with metalloradical character were then isolated and structurally characterized by single crystal X-ray (lab source and synchrotron radiation) diffraction analysis, UV/Vis, and EPR spectroscopy.

## Results and Discussion

1,2-Bis(2,5-dimethylthiophen-3-yl)ethane-1,2-dione (**1**) reacts with an equimolar amount of vanadium(II)bis-$N,N,N',N'$-tetramethylethylenediamine-dichloride ([V(TMEDA)$_2$Cl$_2$], **2**) to give the vanadium(IV) enantiomeric species [V(DTE$_{(apM)}$)$_2$TMEDA] **3**($M,M$) and [V(DTE$_{(apP)}$)$_2$TMEDA] **3**($P,P$) (Scheme 2). It must be noted that the conversion of **1** to the en-diolato ligand is a two-electron reduction. Therefore half of the vanadium must lead to a side product, presumably a "VCl$_4$" chlorido species, which was not further investigated. The racemic mixture **3**($M,M/P,P$) was isolated as a deep blue micro-crystalline solid in 43% yield with respect to starting material **2**. In 1998, Rehder and co-workers gave structural precedence to a non-oxido bisenolato complex of vanadium(IV). Specifically, the redox reaction of compound **2** and benzil was reported to give the corresponding bis benzoin vanadium(IV) complex [V(Ph(O)C=C(O)Ph)$_2$(TMEDA)].[42] We applied a similar synthesis strategy; the V$^{II}$ compound **2** serves as both metal precursor complex and reducing agent for the redox-active ligand precursor **1**. Therefore, the 1,2 diketone motif in **1** is reduced to an enediolate, which is stabilized upon coordination to a vanadium(IV) center to form the non-oxido en-diolato complex **3**($M,M/P,P$). Thus, a hexatrien motif is formed which is a prerequisite for a (reversible) 6π peri-cyclic reaction. Consistently, the cyclic voltammogram of **1** in THF reveals a quasi-reversible redox-wave at a half potential of $E^1_{1/2} = -1.93$ V with respect to the ferrocene/ferrocenium (Fc/Fc$^+$) redox couple. However, although the voltammogram suggests a reversible process for the first redox step, the second redox process is observed at very low potential ($E^2_{red} = -2.80$ V and $E^2_{ox} = -2.63$ V) and is not fully reversible (see Figure 1).

To the best of our knowledge, no five-membered metallacycle with a dithienylethene (DTE) backbone has been reported to date. The compounds entail two axially chiral en-diolato li-
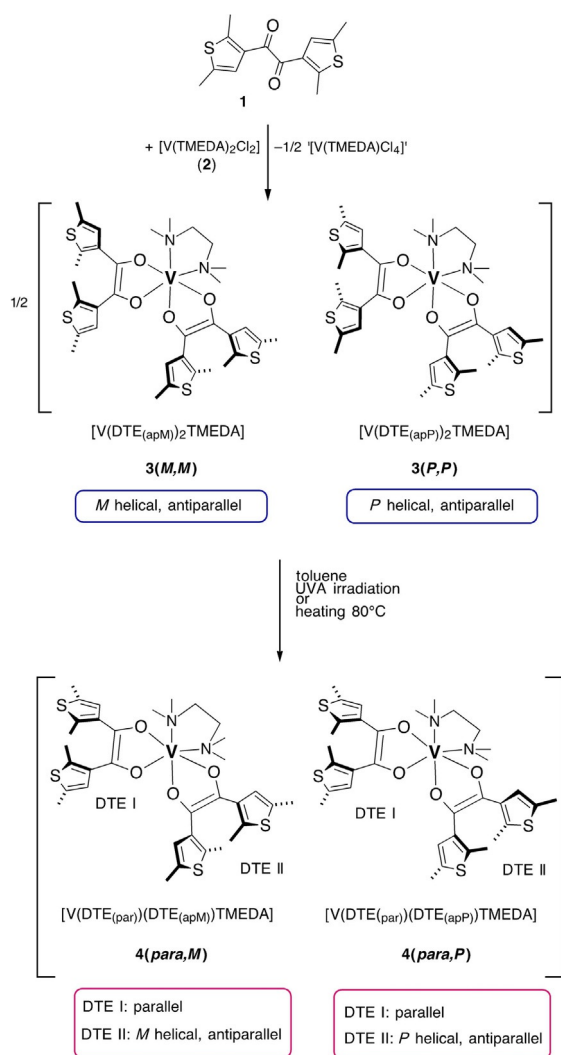
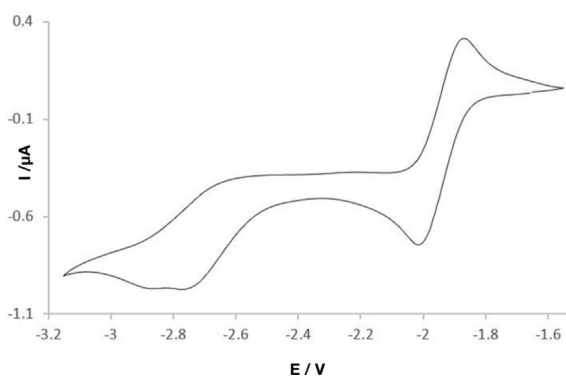**Scheme 2.** Synthesis of the racemic vanadium(IV) compounds **3(M,M/P,P)** and **4(para,M/para,P)**.



**Figure 1.** Cyclic voltammogram of **1** (3.9 mM) at 298 K, in 0.1 M [TBA]PF$_6$ in THF, scan rate 100 mV s$^{-1}$, referenced to Fc/Fc$^+$. Quasi-reversible redox wave at half potential $E^1_{1/2} = -1.93$ V; $E^2_{ox} = -2.60$ V, $E^2_{red} = -2.80$ V.

gands with both DTE ligands in each enantiomer exhibiting antiparallel configurations with *M,M* helicity **3(M,M)** and *P,P* helicity **3(P,P)**. Upon irradiation of crystalline **3(M,M/P,P)** dissolved in toluene with UVA light ($\lambda_{max} = 370$ nm) or prolonged heating of

a toluene solution at 80 °C, the racemate **3(M,M/P,P)** is converted to the closely related [V(DTE$_{(par)}$)(DTE$_{(apM)}$)TMEDA] **4(para,M)** and [V(DTE$_{(par)}$)(DTE$_{(apP)}$)TMEDA] **4(para,P)**. Each of the formed enantiomers exhibits one DTE ligand in an open parallel arrangement and one DTE ligand in an antiparallel arrangement with the respective *M*-helical **4(para,M)** or *P*-helical **4(para,P)** configuration. The isomerization reaction is not reversible and is characterized by a significant color change from deep blue to purple (images are shown in Figure 3). The reaction can be followed in situ in consecutively recorded UV/Vis absorption spectra of crystalline **3(M,M/P,P)** in toluene under concomitant irradiation with UVA light as shown in Figure 2.
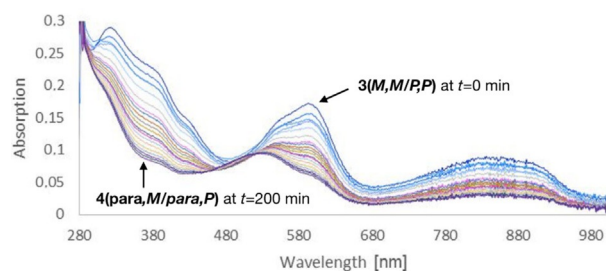


**Figure 2.** Stacked UV/Vis spectra of complex **3(M,M/P,P)** (0.1 mM single crystals dissolved in toluene) under irradiation of UVA light $\lambda_{max} = 370$ nm for $t = 0$–200 min (10 min interval) results in the formation of **4(para,M/para,P)**.

The characteristic shoulder at 593 nm associated with **3(M,M/P,P)** starts to decrease upon irradiation, as well as a decrease in intensity for the strong absorption band at 836 nm and for the signal in the range of 315–430 nm can be observed. After 200 min, the racemic mixture **4(para,M)/4(para,P)** is formed as the major component. In this regard, it is worth noting that photochromic DTE motifs in switchable transition-metal complexes commonly feature the coordination site rather remotely located from the DTE moiety.[43] For instance, Wing-Wah Yam,[44] Bielawski[45,46] and co-workers reported the incorporation of the photochromic DTE motif in the backbone of an N-heterocyclic carbene. The coordination of such a NHC ligand to Rh$^I$ was reported by Bielawski and co-workers to possess switchable catalytic properties in alkene and alkyne hydroborations, which are triggered by the photoinduced reversible cyclization of the DTE motif.[47] Recently, the same group described a photoswitchable olefin metathesis catalyst using a similar NHC ligand.[48] Photochromic and luminescence switching properties of a Re$^I$ triscarbonyl complex with dithienylphenanthroline were published by Wing-Wah Yam, Phillips and co-workers.[49,50] However, non-switching coordination complexes with DTE entities were reported for which no cyclization reaction was observed.[51]

## Single-crystal X-ray diffraction analysis

The racemic mixture of compound **3(M,M/P,P)** crystallizes in the monoclinic centrosymmetric space group $P2_1/n$. Therefore, both enantiomers are present in equal amount in the unit cell, that is, the two DTE ligands in each enantiomer are either in

an antiparallel *M*-helical **3(*M,M*)** or antiparallel *P*-helical **3(*P,P*)** arrangement with respect to the assignment of the highest priority to the methyl groups. Single crystals suitable for X-ray diffraction analysis were obtained by slow diffusion of *n*-pentane into a THF solution of **3(*M,M/P,P*)**. The determined molecular structure is shown for complex **3(*M,M*)** in Figure 3, top left. The structure reveals the vanadium metal center in an octahedral coordination sphere, which consists of four oxygen donors associated with two bidentate DTE en-diolato ligands and the two nitrogen donors of the TMEDA ligand. The en-diolate motif is characterized by short C=C double bonds (C7–C8 = 1.369(7) Å and C21–C22 = 1.365(7) Å) and O–C single bonds (O1–C7 = 1.330(5) Å; O2–C8 = 1.345(5) Å and O3–C21 = 1.344(5) Å; O4–C22 = 1.349(6) Å) suggesting two dianionic en-diolato ligand motifs coordinated to a formal vanadium(IV) center. Most significantly, due to a restricted rotation about the C–C bond connecting the thiophene units and the ethylene backbone, both DTE ligands in complex **3(*M,M/P,P*)** bear axial chirality and the enantiomeric complexes are atropisomers. Multiple attempts to grow single crystals of **4(*para,M/ para,P*)** suitable for an X-ray diffraction study proved to be difficult due to the extraordinarily small size of the crystals obtained. This prompted us to undertake an X-ray diffraction study by using a synchrotron radiation source (beamline BL02B1 at SPring-8, Japan). A representative molecular structure is shown in Figure 3 top, right [**4(*para,M*)**]. The racemic mixture **4(*para,M/para,P*)** crystallizes in the monoclinic centrosymmetric space group $P2_1/c$ with both enantiomers present in the unit cell. The molecular structures of **4(*para,M/para,P*)** exhibit similar interatomic distances around the vanadium center and in the en-diolato backbone with respect to **3(*M,M/ P,P*)** [C=C double bond (C7–C8 = 1.366(7) Å and C21–C22 = 1.368(7) Å) and O–C single bonds (O1–C7 = 1.349(6) Å; O2–C8 = 1.339(6) Å and O3–C21 = 1.345(6) Å; O4–C22 = 1.351(5) Å)]. However, the structure unambiguously indicates a change to the parallel configuration in only one of the DTE ligands due to a rotation about the C–C bond connecting the thiophene rings and en-diolato backbone. The other DTE unit retains its corresponding antiparallel *M* or *P* helicity to give the enantiomers **4(*para,M*)** and **4(*para,P*)**, respectively. An overlay plot of the blue compound **3(*M,M*)** and purple compound **4(*para,M*)** is shown in Figure 3, bottom. The crystallographic investigation of single crystals of **3(*M,M/P,P*)** and **4(*para,M/ para,P*)** allows for the unambiguous structural characterization of the four atropisomers.
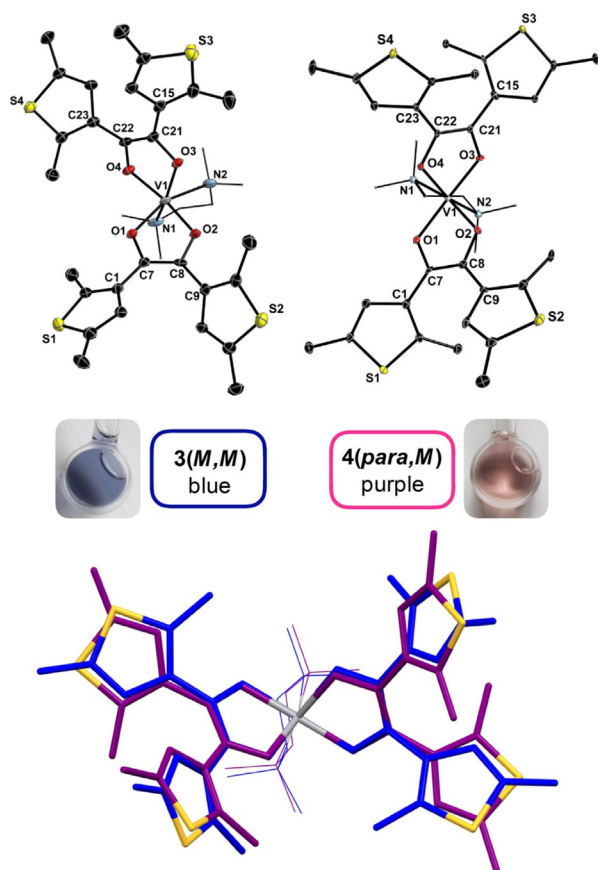
## EPR spectroscopic study

With the aim of gaining insight into the solution structure, the blue **3(*M,M/P,P*)** and purple **4(*para,M/para,P*)** compounds were investigated by dissolving crystalline samples in THF. We cannot exclude isomerization upon dissolution, however, both solutions exhibit the characteristic blue and purple color, respectively. Both samples give similar but distinctly different EPR spectra as shown in Figure 4, which indicates the existence of two (or more) atropisomers. All experimental EPR spectra indicate metal-centered radicals, that is, $V^{IV}$ metalloradicals. The purple solution spectrum at both room temperature and in frozen-solution is accurately simulated with a single EPR component denoted **4**. These data were modelled with an electron Zeeman (principal *g* values $g_1$, $g_2$, $g_3$) and a $^{51}$V hyperfine ($A_1$, $A_2$, $A_3$) interaction with the isotropic values $g_{iso}$ and $A_{iso}$ used for the room temperature spectrum being the average of the three principal values of the corresponding interaction, for example, $g_{iso} = (g_1 + g_2 + g_3)/3$ and $A_{iso} = (A_1 + A_2 + A_3)/3$.

The blue solution was more complicated. Accurately simulating its isotropic room temperature spectrum requires a two component EPR model comprising of the same component **4** as observed in the purple solution and a new EPR component denoted **3** which again was modelled by an isotropic *g* value and isotropic vanadium hyperfine coupling (Table 1). In the room temperature spectrum, the two resolved EPR components have the relative weighting $0.54 \times \mathbf{3}^{RT} + 0.46 \times \mathbf{4}$. However, in frozen solution there are at least three EPR components resolved as can be deduced by examination of the high-field feature in the CW EPR spectrum that arises from the largest



**Figure 3.** Top: Mercury plot of exemplary complex **3(*M,M*)** (left) and **4(*para,M*)** (right) at 50% ellipsoid probability. Bottom: Wireframe structural overlap of **3(*M,M*)** (blue) and **4(*para,M*)** (purple). Hydrogen atoms are omitted for clarity. Selected bond lengths [Å]: **3(*M,M*)**: C1–C7 = 1.473(6), C7–C8 = 1.369(7), C8–C9 = 1.467(6), O1–C7 = 1.330(5), O2–C8 = 1.345(5), C15–C21 = 1.481(7), C21–C22 = 1.365(7), C22–C23 = 1.473(7), O3–C21 = 1.344(5), O4–C22 = 1.349(6), V–N1 = 2.238(5), V1–N2 = 2.200(5). **4(*para,M*)**: C1–C7 = 1.475(7), C7–C8 = 1.366(7), C8–C9 = 1.471(7), O1–C7 = 1.349(6), O2–C8 = 1.339(6), C15–C21 = 1.476(7), C21–C22 = 1.368(7), C22–C23 = 1.472(6), O3–C21 = 1.345(6), O4–C22 = 1.351(5), V–N1 = 2.195(5), V–N2 = 2.215(5).
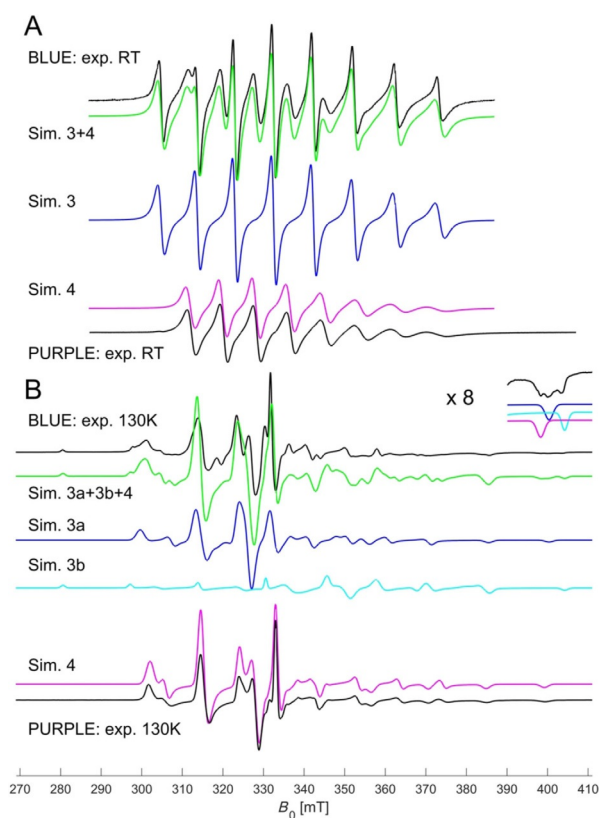
**Figure 4.** X-band (9.3810 GHz) CW EPR spectra measured at room temperature (A) and at 130 K (B) for the blue and purple solutions in THF. Simulated EPR model components and the sum are shown next to each experimental spectrum.
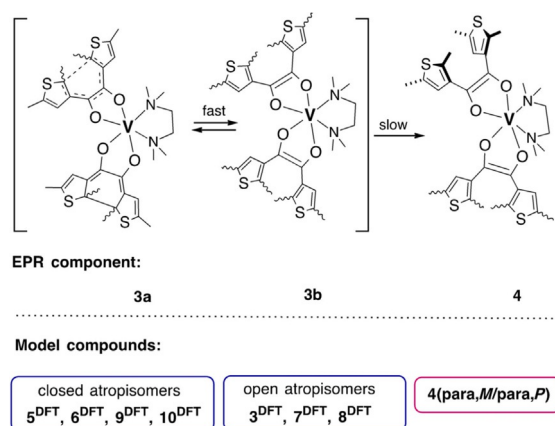
**Table 1.** EPR parameters for the blue and purple samples derived from experimental and DFT data. Simulation of the CW EPR spectra provide for each component the principal $g$ values, $^{51}$V hyperfine couplings (MHz), linewidth (MHz), and for room temperature data, the rotational correlation time $\tau_R$ (ns). For the DFT geometry optimized structures EPR parameters are computed ($g$ values and $^{51}$V hyperfine couplings) and compared to the experimental parameters.

| EPR parameters | | Principal values | Isotropic |
|---|---|---|---|
| **"Purple" component** | | | |
| Model **4** | $g$ | 1.9114, 1.9694, 1.9886 | 1.9564 |
| | $^{51}$V[a] | −371, −268, −69 | −236 |
| | LW | 58, 42, 23 | |
| | $\tau_R$ | 0.14 | |
| **4**$^{DFT}$(*para,M/para,P*) | $g$ | 1.9276, 1.9682, 1.9757 | 1.9571 |
| | $^{51}$V | −365, −226, −81 | −224 |
| | | | |
| **"Blue" component** | | | |
| Model **3**$^{RT}$ (RT) | $g$ | NA | 1.9735 |
| | $^{51}$V[a] | NA | −271.8 |
| | LW | NA | – |
| | $\tau_R$ | NA | 0.44 |
| Model **3a** (130 K) | $g$ | 1.910, ≈1.97, ≈1.98 | ND |
| | $^{51}$V[a] | −385, ≈−260, ≈−70 | ND |
| | LW | 57, 42, 30 | ND |
| Model **3b** (130 K) | $g$ | ≈1.92, ≈1.94, 1.970[b] | ND |
| | $^{51}$V[a] | ≈−260, ≈−250, −475 | ND |
| | LW | 57, 42, 30 | ND |
| | | | |
| **DFT optimized structures** | | | |
| **3**$^{DFT}$(*M,M/P,P*) | $g$ | 1.9276, 1.9670, 1.9730 | 1.9560 |
| | $^{51}$V | −363, −232, −92 | −167 |
| **5**$^{DFT}$(*M,closed-S,S*) | $g$ | 1.9083, 1.9377, 1.9752[c] | 1.9404 |
| | $^{51}$V | −131, −306, −413 | −283 |
| **6**$^{DFT}$(*closed-S,S,closed-S,S*) | $g$ | 1.9160, 1.9357, 1.9640[c] | 1.9385 |
| | $^{51}$V | −308, −223, −498 | −343 |
| **7**$^{DFT}$(*M,P*) | $g$ | 1.9345, 1.9530, 1.9629 | 1.9501 |
| | $^{51}$V | −390, −198, −270 | −286 |
| **8**$^{DFT}$(*para,para*) | $g$ | 1.9284, 1.9674, 1.9749 | 1.9570 |
| | $^{51}$V | −365, −224, −85 | −225 |
| **9**$^{DFT}$(*closed-R,R,closed-S,S*) | $g$ | 1.9149, 1.9328, 2.0386 | 1.9621 |
| | $^{51}$V | −156, −323, −435 | −305 |
| **10**$^{DFT}$(*P,closed-S,S*) | $g$ | 1.8989, 1.9400, 1.9887 | 1.9425 |
| | $^{51}$V | −109, −306, −431 | −282 |

[a] CW EPR only determines the absolute values of the hyperfine coupling; the sign was set according to the DFT data. [b] Principal $g$ values and $^{51}$V hyperfine coupling not collinear, the hyperfine interaction in the $g$-matrix frame is given as A = R*A$_{diagonal}$*R$^T$, in which $R$ = [0.5121611 0.0082016 −0.8588503; −0.0021891 0.9999636 0.0082437; 0.8588866 −0.0023421 0.5121604]. [c] Principal $g$ values and $^{51}$V hyperfine coupling not collinear. NA = not available; ND = not defined.

principal value of the $^{51}$V hyperfine interaction, see the blowup of the region around 400 mT in Figure 4B. The appearance of three resolved features indicates the presence of three resolved EPR components. The observation of only two components at room temperature in the blue solution may be because of the presence of several species that interconvert rapidly in solution at room temperature to give an average spectrum **3**$^{RT}$, whereas in frozen-solution the individual components of this average are observed. In the simulation of the frozen-solution data, these components are denoted **3a** and **3b**. It must be noted that EPR component **4** does not appear to be involved in any room temperature averaging process as it is present in both the room temperature and frozen-solution data. A reasonable model for the blue spectrum was obtained with a simulation employing three EPR components (**3ab**, **4**) with approximately equal relative weights. Spin Hamiltonian parameters for all EPR model components are listed in Table 1. It must be noted that the largest hyperfine value of **3a** and **3b** is accurately determined but the other $g$ and $A$ values are estimates because they are difficult to determine given the complexity of the spectrum particularly in terms of EPR component number. For example, component **3b** accurately accounts for the largest $^{51}$V hyperfine coupling observed in the experiment with its spectrum ranging from 280 to 403 mT, a range quite distinct from **3a** and **4**.

To help assign the EPR components **3a**, **b** and **4** to a chemical structure, various models were tested. For each structural model, density functional theory (DFT) was used to obtain a geometry optimized structure which was subsequently used to compute EPR parameters for comparison to the experimental data as shown in Table 1. The optimized geometries are listed in the Supporting Information. The DFT computed EPR parameters for the structure of the model **4**(*para,M/para,P*) fit the EPR parameters from the purple solution very accurately (Table 1) and, thus, allow EPR component **4** to be assigned to atropisomer **4**(*para,M/para,P*) with metalloradical character in solution. However, assignment of the EPR components **3a** and

**3b** from the blue solution on the basis of the EPR parameters (g values and $^{51}$V hyperfine couplings) was not as definitive as for **4**. Seven structural models were investigated: The model for compound **3**(*M,M/P,P*) and the (partially) closed compounds **5**$^{DFT}$(*M,closed-S,S*), **6**$^{DFT}$(*closed-S,S,closed-S,S*) **9**$^{DFT}$(*closed-R,R,closed-S,S*), and **10**$^{DFT}$(*P,closed-S,S*), in which the DTE moiety underwent a pericyclic ring closure. Model **7**$^{DFT}$(*M,P*) has two DTE ligands with *M* and *P* helicity, respectively. Structural model **8**$^{DFT}$(*para,para*) carries both DTE ligands in a parallel alignment. Component **3b** exhibits a large and well determined $^{51}$V principal hyperfine coupling value of $A_3(^{51}V) = -475$ MHz, which is best matched by the group of (partially) closed compounds **5**$^{DFT}$(*M,closed-S,S*), **6**$^{DFT}$(*closed-S,S,closed-S,S*), **9**$^{DFT}$(*closed-R,R,closed-S,S*), and **10**$^{DFT}$(*P,closed-S,S*) with $A_3^{DFT}(^{51}V)$ ranging from $-413$ to $-498$ MHz. The other models all have significantly lower largest $A^{DFT}(^{51}V)$ values in the 300 MHz range. On this basis, EPR component **3b** is tentatively assigned to a compound class bearing cyclized DTE ligands. Component **3a** has $A_3(^{51}V) = -385$ MHz and given the limited experimental accuracy of the other *A* and *g* principal values, the signal could arise from a compound with both DTE in their non-cyclized form such as in **3**$^{DFT}$(*M,M/P,P*), **7**$^{DFT}$(*M,P*) or **8**$^{DFT}$(*para,para*) (see Scheme 3). These three DFT models all have similar *A* and *g* values. Given the complexity of the experimental spectrum, we cannot rule out either that a combination of EPR components with slightly different EPR parameters are required to accurately explain the **3b** CW EPR signals.



**EPR component:**

3a          3b          4

**Model compounds:**

| closed atropisomers | open atropisomers | 4(para,*M*/para,*P*) |
| **5**$^{DFT}$, **6**$^{DFT}$, **9**$^{DFT}$, **10**$^{DFT}$ | **3**$^{DFT}$, **7**$^{DFT}$, **8**$^{DFT}$ | |

**Scheme 3.** Dynamic interconversion of EPR components **3ab** and **4** in solution and assignment of DFT models.

## Conclusion

The redox-active ligand 1,2-bis(2,5-dimethylthiophen-3-yl)-ethane-1,2-dione (**1**) reacts with [V(TMEDA)$_2$Cl$_2$] (**2**) in a disproportionation reaction to give rare non-oxido vanadium(IV) species encompassing two bis-enolato ligands with 1,2-dithienyl-ethene (DTE) backbone. A blue crystalline product was isolated from the reaction mixture. Upon irradiation with a UVA-light source or heating of a toluene solution, a color change occurs from blue to purple and a purple crystalline material was obtained from the solution. Our single-crystal XRD analysis of

both isolated compounds reveals the structure of the racemic complex **3**(*M,M/P,P*) (blue) and **4**(*para,M/para,P*) (purple). The antiparallel configuration of the thiophene rings of the DTE ligands in both complexes display axial chirality corresponding to *M* or *P* helicity. A parallel configuration is observed in complex **4**(*para,M/para,P*).

The vanadium(IV) center is chelated through the en-diolate of each DTE ligand giving rise to five-membered metallacycles with a hexatriene motif formed in the DTE scaffold. The antiparallel alignment present in both **3**(*M,M/P,P*) and **4**(*para,M/para,P*) is a prerequisite for potential (reversible) 6π cyclization reactions (Scheme 1) and thus for the development of for example, photoswitchable metalloradicals.

With the aim of characterizing the solution structures, X-band CW EPR spectra were recorded of solutions of crystalline samples of **3**(*M,M/P,P*) and **4**(*para,M/para,P*) dissolved in THF at room temperature and in frozen solution. All obtained EPR spectra indicate vanadium-centered radicals. The purple solution spectrum of **4**(*para,M/para,P*) at both room temperature and in frozen-solution contained a single EPR-active component **4**, which is assigned to **4**(*para,M/para,P*). The X-band EPR solution spectrum of the blue **3**(*M,M/P,P*) indicates a complex dynamic behavior; two EPR components are resolved at room temperature comprising of **4** and another denoted **3**$^{RT}$. We assume that **3**$^{RT}$ is an average spectrum of rapidly interconverting species as there are three (or more) components in the frozen-solution spectrum (including **4**). The frozen-solution spectrum was modelled by **4** and components **3a** and **3b**. Although **3b** may be described as a complex with one or two cyclized DTE units represented by model compounds **5**$^{DFT}$, **6**$^{DFT}$, **9**$^{DFT}$, or **10**$^{DFT}$, component **3a** is best described as a complex involving only open DTE units represented here by model compounds **3**$^{DFT}$, **7**$^{DFT}$, or **8**$^{DFT}$ or a combination thereof (see Scheme 3). Component **4** does not appear to be involved in dynamic averaging processes as **4** is definitively detected at room temperature as well as in frozen solution. Compound **4** thus appears to be the thermodynamically stable atropisomer because it forms slowly from **3**(*M,M/P,P*) solutions. The formation of the blue component **3** is kinetically controlled in the course of the synthesis of **3**(*M,M/P,P*) starting from ligand precursor **1** and complex **2**.

In conclusion, switchable transition-metal complexes bearing photochromic DTE motifs commonly have the coordination site rather distant from the DTE backbone and its hexatriene system. Here, we report the bidentate en-diolato ligand **F**, which directly chelates V$^{IV}$ centers giving rise to five-membered metallacycles with adjacent DTE hexatriene backbone. Although we do not observe well-defined photochemically triggered cyclization, we found evidence for dynamic reversible cyclization reactions starting from **3**(*M,M/P,P*) at ambient temperature in solution.

## Experimental Section

### Crystallographic data

**Experimental details for single crystal X-ray diffraction analysis of complexes 3(*M*,*M*/*P*,*P*) and 4(para,*M*/para,*P*)**: Diffraction experiments were performed on a Bruker D8 Venture in-house diffractometer using $Mo_{K\alpha}$ radiation and at the beamline BL02B1 of SPring-8 in Hyogo, Japan, using a wavelength of 0.3567 Å. The collection of the dataset of compound 4(para,*M*/para,*P*) was done under exclusion of light and oxygen by using argon atmosphere while preparing crystals. Further details are shown in Table 2 and in the crystallographic information files (CIFs) deposited with the Cambridge Structural Database. CCDC 1946375 and 1946376 contain the supplementary crystallographic data for this paper. These data are provided free of charge by The Cambridge Crystallographic Data Centre.

**Table 2.** Details on the measurements and refinements of compound 3(*M*,*M*/*P*,*P*) and 4(para,*M*/para,*P*).

| Structure | 3(*M*,*M*)/(*P*,*P*) | 4(para,*M*)/(para,*P*) |
|---|---|---|
| Sum formula | $C_{34}H_{44}N_2O_4S_4V$ | $C_{34}H_{44}N_2O_4S_4V$ |
| Mol. mass (g mol$^{-1}$) | 723.89 | 723.89 |
| Space group | $P2_1/n$ | $P2_1/c$ |
| $a$ [Å] | 10.4187(5) | 28.109(6) |
| $b$ [Å] | 25.2837(11) | 8.9569(18) |
| $c$ [Å] | 13.8148(7) | 14.529(3) |
| $\beta$ [°] | 108.345(2) | 94.47(3) |
| $V$ [Å$^3$] | 3454.2(3) | 3646.8(13) |
| $Z$ | 4 | 4 |
| $F_{000}$ | 1524 | 1524 |
| Radiation | Mo-$K_\alpha$ (0.71073 Å) | Synchr. (0.3567 Å) |
| $T$ [K] | 100(1) | 20(1) |
| Crystal color | blue | purple |
| Diffractometer | Bruker D8 Venture | SPring-8 Rigaku CCD |
| Max. resolution [Å] | 0.82 | 0.75 |
| $R_{int}$ | 0.089 | 0.173 |
| $hkl$ (−min=max) | 12/30/16 | 37/11/19 |
| # of reflns | 35517 | 63595 |
| # of indep. reflns | 6455 | 9032 |
| $R$ | 0.064 | 0.089 |
| w$R$(F$^2$) | 0.131 | 0.188 |
| GoF | 1.14 | 1.11 |
| Residual [e Å$^{-3}$] | 0.60/−0.38 | 1.14/−0.73 |
| Obsv. criteria | $F^2 > 2\sigma(F^2)$ | $F^2 > 2\sigma(F^2)$ |
| CCDC entry[a] | 1946375 | 1946376 |

[a] See also the Experimental Section.

### Method and materials

If not mentioned otherwise, all reactions were carried out in a heavy-walled Schlenk tube with a wide bore Teflon screw stopcock under an atmosphere of dry argon. Solvents and chemicals were used without further purification.

**UV/Vis spectroscopy**: Experiments were carried out at 298 K on a Varian Cary 50 UV/Vis spectrophotometer. Cuvettes: 10 mm, synthetic quartz (QS) with Teflon cap. Probes were prepared under an inert atmosphere of argon.

**Cyclic voltammetry**: Experiments were carried out at 298 K with a Metrohm potentiostat running the NOVA 2.1 software package using a RHD Instruments electrochemical cell TSC 1600 closed. Solvent: THF; Electrolyte: [TBA]PF6; Electrodes: Pt working electrode, Ag/AgCl pseudo reference electrode, Pt counter electrode.

**Continuous-wave (CW) electron paramagnetic resonance**: X-band (9.3810 GHz) CW EPR measurements were carried out on a Bruker ElexSys E540 spectrometer equipped with a Bruker super-high-Q cavity and a Eurotherm LN$_2$ cooling system. Room temperature measurements were made under non-saturating conditions using a microwave power of 20 mW with a modulation frequency of 100 KHz and a modulation amplitude of 0.1 mT. Measurement in frozen solution used a microwave power of 5.0 mW (non-saturating) with a modulation frequency of 100 KHz and modulation amplitude of 0.3 mT. The spectrometer field was calibrated with 2,2-diphenyl-1-picrylhydrazyl (DPPH: $g = 2.0036$). Simulations used the XSophe[52] and Easyspin[53] software.

**Density functional theory**: Calculations to compute EPR parameters were performed using ORCA 3.0.3.[54,55] Geometry optimization was performed using the UKS B3LYP functional, a T2V basis set and a frozen core for all electrons, and a COSMO model for THF. The g-, hyperfine and nuclear quadrupole tensors were calculated using a spin-unrestricted Kohn–Sham self-consistent field calculation method with a ZORA scalar relativistic Hamiltonian and the B3LYP functional, using the Def2QZVPP basis set for V and the def2TZVPP basis set for all other nuclei,[56] and tighter convergence constraints. The spin-orbit coupling was calculated using the SOMF(1X) option in ORCA.

### Synthetic protocols

**[V$_2$($\mu$-Cl)$_3$(THF)$_6$]$_2$[Zn$_2$Cl$_6$]**: the compound was prepared following a slightly modified literature procedure:[57] 1) **VCl$_3$(THF)$_3$**: VCl$_3$ (0.50 g, 3.18 mmol, 1.00 equiv) was suspended in THF (40 mL) and stirred for 48 h at 75 °C. The formed light purple solution was subsequently filtered and the solvent removed under reduced pressure. Yield: 1.18 g (3.15 mmol, 99%). 2) **VCl$_3$(THF)$_3$** (1.00 g, 2.68 mmol, 1.00 equiv), dissolved in THF (50 mL), was treated with zinc powder (0.44 g, 6.69 mmol, 2.50 equiv) and stirred for 48 h at room temperature. After removal of the solvent under reduced pressure, the green product was dissolved in DCM, filtered, dried and washed with small portions of *n*-pentane. Yield: 0.87 g (0.54 mmol, 80%).

**VCl$_2$(TMEDA)$_2$**: the compound was prepared following a modified literature procedure:[58] [V$_2$($\mu$-Cl)$_3$(THF)$_6$]$_2$[Zn$_2$Cl$_6$] (0.70 g, 0.43 mmol, 1.00 equiv) was suspended in THF (30 mL), treated with *N,N,N′,N′*-tetramethylethylenediamine (2.3 mL, 15.07 mmol, 35.00 equiv), stirred at 75 °C for 6 h and then at room temperature for 16 h. After partial removal of the solvent under reduced pressure, blue crystals separated from the red solution upon standing overnight in a cryostat at 5 °C. The supernatant was decanted and the product washed with small portions of cold THF. Yield: 0.53 g (1.51 mmol, 87%).

**1,2-Bis(2,5-dimethylthiophen-3-yl)ethane-1,2-dione (DTE, 1)**: the compound was prepared following a modified literature procedure:[59] In a three neck flask, AlCl$_3$ (9.39 g, 70.42 mmol, 1.00 equiv) was suspended in DCM (40 mL), cooled to −15 °C and treated with pyridine (2.8 mL, $\rho = 0.978$ g cm$^{-3}$, 35.21 mmol, 0.50 equiv) and 2,5-dimethylthiophene (8.0 mL, $\rho = 0.985$ g cm$^{-3}$, 70.42 mmol, 1.00 equiv), each dissolved in DCM (40 mL). Over a time period of 40 minutes, oxalyl chloride (3.6 mL, $\rho = 1.48$ g cm$^{-3}$, 42.25 mmol, 0.60 equiv), dissolved in CH$_2$Cl$_2$ (40 mL), was added to the red solution. After stirring for 40 min at −5 °C and 1 h at 5–10 °C, the mixture was poured onto ice. The organic layer was separated and the aqueous layer extracted with chloroform. The combined organic phases were then washed with water, sodium carbonate solution and saturated NaCl solution subsequently. Filtering through hot

cotton and removal of the solvent under reduced pressure was followed by flash chromatography (cyclohexane/ethylacetate, 100:3) of the viscous oil and led to pure orange-brown product. Yield: 4.12 g (14.80 mmol, 42%), $R_f = 0.38$.

**[V(DTE(apM))₂TMEDA]/ [V(DTE(apP))₂TMEDA] (3(M,M/P,P)):** Compound **1** (0.20 g, 0.71 mmol, 1.00 equiv) was added to a suspension of [VCl₂(TMEDA)₂] (0.25 g, 0.71 mmol, 1.00 equiv) in THF (15 mL). The resulting dark-blue solution was stirred at 75 °C for 24 h. After filtration and partial removal of the solvent under reduced pressure, *n*-pentane was allowed to diffuse into the saturated solution for seven days, allowing for the crystallization of product **3**. The supernatant was decanted and the product was washed with small portions of *n*-pentane and subsequently dried in a stream of argon. Yield: 0.22 g (0.30 mmol, 43%).

**[V(DTE(par))(DTE(apM))TMEDA]/[V(DTE(par))(DTE(apP))TMEDA]**

**[4(para,M/para,P)]:** *Photochemical isomerization*: In a typical experiment, a 20 mL fused-quartz Schlenk tube with Teflon valve was charged with a toluene solution of compound **3(M,M/P,P)** (0.01–0.02 mм). The sample was irradiated with UVA light ($\lambda_{max} = 370$ nm), performed in a custom-built photoreactor with two 11 W UVA lamps (Philips UV-A PL-S 11 W/10/2P, 28 mm diameter, 236 mm total length) equipped with a cooling ventilator. Distance to probe: 10 cm. The reaction is characterized by a color change from deep blue to purple. The solvent was removed under reduced pressure after 4–6 h reaction time. The product was isolated as purple powder in quantitative yield. Crystals suitable for single-crystal X-ray diffraction analysis by using synchrotron radiation at the BL02B1 beamline at SPring-8 in Hyogo, Japan, were obtained from a saturated solution of **4(para,M/para,P)** in toluene upon standing for several days. *Thermal isomerization:* A toluene solution of **3(M,M/P,P)** (0.1–0.2 mм) was transferred in a Schlenk tube with a wide bore Teflon screw stopcock and heated to 80 °C for 12 h. The reaction is characterized by a color change from deep blue to purple. The supernatant was removed in vacuo leaving compound **4(para,M/para,P)** as a purple solid.

## Conflict of interest

The authors declare no conflict of interest.

[1] D. C. Crans, J. J. Smee, E. Gaidamauskas, L. Yang, *Chem. Rev.* **2004**, *104*, 849–902.

[2] J. Costa Pessoa, E. Garribba, M. F. A. Santos, T. Santos-Silva, *Coord. Chem. Rev.* **2015**, *301–302*, 49–86.

[3] K. H. Thompson, J. H. McNeill, C. Orvig, *Chem. Rev.* **1999**, *99*, 2561–2572.

[4] K. H. Thompson, J. Lichter, C. LeBel, M. C. Scaife, J. H. McNeill, C. Orvig, *J. Inorg. Biochem.* **2009**, *103*, 554–558.

[5] Y. Wei, C. Zhang, P. Zhao, X. Yang, K. Wang, *J. Inorg. Biochem.* **2011**, *105*, 1081–1085.

[6] D. Sanna, G. Micera, E. Garribba, *Inorg. Chem.* **2013**, *52*, 11975–11985.

[7] M. Sutradhar, L. M. D. R. S. Martins, M. F. C. Guedes da Silva, A. J. L. Pombeiro, *Coord. Chem. Rev.* **2015**, *301–302*, 200–239.

[8] E. Amadio, R. Di Lorenzo, C. Zonta, G. Licini, *Coord. Chem. Rev.* **2015**, *301–302*, 147–162.

[9] D. Rehder, *Dalton Trans.* **2013**, *42*, 11749–11761.

[10] a) G. H. Spikes, S. Sproules, E. Bill, T. Weyhermüller, K. Wieghardt, *Inorg. Chem.* **2008**, *47*, 10935–10944; b) S. Sproules, T. Weyhermüller, S. DeBeer, K. Wieghardt, *Inorg. Chem.* **2010**, *49*, 5241–5261.

[11] R. E. Berry, E. M. Armstrong, R. L. Beddoes, D. Collison, S. N. Ertok, M. Helliwell, C. D. Garner, *Angew. Chem. Int. Ed.* **1999**, *38*, 795–797; *Angew. Chem.* **1999**, *111*, 871–873.

[12] E. Bayer, H. Kneifel, *Z. Naturforschung Sect. B* **1972**, *27*, 207.

[13] D. Sanna, V. Ugone, G. Micera, T. Pivetta, E. Valletta, E. Garribba, *Inorg. Chem.* **2015**, *54*, 8237–8250.

[14] M. Irie, T. Fukaminato, K. Matsuda, S. Kobatake, *Chem. Rev.* **2014**, *114*, 12174–12277.

[15] M. Irie, *Proc. Jpn. Acad. Ser. B* **2010**, *86*, 472–483.

[16] M. Irie, *Photochem. Photobiol. Sci.* **2010**, *9*, 1535–1542.

[17] C. Yun, J. You, J. Kim, J. Huh, E. Kim, *J. Photochem. Photobiol. C* **2009**, *10*, 111–129.

[18] C. P. Harvey, J. D. Tovar, *Polym. Chem.* **2011**, *2*, 2699–2706.

[19] S.-Z. Pu, Q. Sun, C.-B. Fan, R.-J. Wang, G. Liu, *J. Mater. Chem. C* **2016**, *4*, 3075–3093.

[20] M. Irie, *Chem. Rev.* **2000**, *100*, 1685–1716.

[21] T. Hirose, K. Matsuda, *Org. Biomol. Chem.* **2013**, *11*, 873–880.

[22] C. Xiao, W.-Y. Zhao, D.-Y. Zhou, Y. Huang, Y. Tao, W.-H. Wu, C. Yang, *Chin. Chem. Lett.* **2015**, *26*, 817–824.

[23] S. Cui, G. Liu, S. Pu, B. Chen, *Dyes Pigm.* **2013**, *99*, 950–956.

[24] D. Frath, S. Yokoyama, T. Hirose, K. Matsuda, *J. Photochem. Photobiol. C* **2018**, *34*, 29–40.

[25] Y. Takagi, M. Morimoto, R. Kashihara, S. Fujinami, S. Ito, H. Miyasaka, M. Irie, *Tetrahedron* **2017**, *73*, 4918–4924.

[26] C. Li, H. Yan, L.-X. Zhao, G.-F. Zhang, Z. Hu, Z.-L. Huang, M.-Q. Zhu, *Nat. Commun.* **2014**, *5*, 5709.

[27] S. Erbas-Cakmak, D. A. Leigh, C. T. McTernan, A. L. Nussbaumer, *Chem. Rev.* **2015**, *115*, 10081–10206.

[28] J. E. Smyth, N. M. Butler, P. A. Keller, *Nat. Prod. Rep.* **2015**, *32*, 1562–1583.

[29] M. Ōki in *Topics in Stereochemistry, Vol. 14* (Eds.: N. L. Allinger, E. L. Eliel, S. H. Wilen), Wiley, New York, **1983**, pp. 1–81.

[30] K. Mikami, M. Yamanaka, *Chem. Rev.* **2003**, *103*, 3369–3400.

[31] L. Pu, *Chem. Rev.* **1998**, *98*, 2405–2494.

[32] F. Leroux, *ChemBioChem* **2004**, *5*, 644–649.

[33] R. Noyori, *Angew. Chem. Int. Ed.* **2002**, *41*, 2008–2022; *Angew. Chem.* **2002**, *114*, 2108–2123.

[34] A. Miyashita, A. Yasuda, H. Takaya, K. Toriumi, T. Ito, T. Souchi, R. Noyori, *J. Am. Chem. Soc.* **1980**, *102*, 7932–7934.

[35] E. Kumarasamy, R. Raghunathan, M. P. Sibi, J. Sivaguru, *Chem. Rev.* **2015**, *115*, 11239–11300.

[36] P. W. Glunz, *Bioorg. Med. Chem. Lett.* **2018**, *28*, 53–60.

[37] J. Clayden, W. J. Moran, P. J. Edwards, S. R. LaPlante, *Angew. Chem. Int. Ed.* **2009**, *48*, 6398–6401; *Angew. Chem.* **2009**, *121*, 6516–6520.

[38] A. Zask, J. Murphy, G. A. Ellestad, *Chirality* **2013**, *25*, 265–274.

[39] M. Fukagawa, I. Kawamura, T. Ubukata, Y. Yokoyama, *Chem. Eur. J.* **2013**, *19*, 9434–9437.

[40] H. Tian, S. Yang, *Chem. Soc. Rev.* **2004**, *33*, 85–97.

[41] M. Walko, Ben L. Feringa, *Chem. Commun.* **2007**, 1745–1747.

[42] M. Farahbakhsh, H. Schmidt, D. Rehder, *Chem. Commun.* **1998**, 2009–2010.

[43] C.-C. Ko, V. W.-W. Yam, *Acc. Chem. Res.* **2018**, *51*, 149–159.

[44] V. W.-W. Yam, J. K.-W. Lee, C.-C. Ko, N. Zhu, *J. Am. Chem. Soc.* **2009**, *131*, 912–913.

[45] B. M. Neilson, V. M. Lynch, C. W. Bielawski, *Angew. Chem. Int. Ed.* **2011**, *50*, 10322–10326; *Angew. Chem.* **2011**, *123*, 10506–10510.

[46] B. M. Neilson, C. W. Bielawski, *J. Am. Chem. Soc.* **2012**, *134*, 12693–12699.

[47] B. M. Neilson, C. W. Bielawski, *Organometallics* **2013**, *32*, 3121–3128.

[48] A. J. Teator, H. Shao, G. Lu, P. Liu, C. W. Bielawski, *Organometallics* **2017**, *36*, 490–497.

[49] C.-C. Ko, W. M. Kwok, V. W.-W. Yam, D. L. Phillips, *Chem. Eur. J.* **2006**, *12*, 5840–5848.

[50] V. W. W. Yam, C.-C. Ko, N. Zhu, *J. Am. Chem. Soc.* **2004**, *126*, 12734–12735.

[51] A. Presa, L. Barrios, J. Cirera, L. Korrodi-Gregorio, R. Perez-Tomas, S. J. Teat, P. Gamez, *Inorg. Chem.* **2016**, *55*, 5356–5364.

[52] G. R. Hanson, K. E. Gates, C. J. Noble, M. Griffin, A. Mitchell, S. Benson, *J. Inorg. Biochem.* **2004**, *98*, 903–916.

[53] S. Stoll, A. Schweiger, *J. Magn. Reson.* **2006**, *178*, 42–55.

[54] F. Neese, *WIREs Comput. Mol. Sci.* **2012**, *2*, 73–78.

[55] a) A. Schäfer, H. Horn, R. Ahlrichs, *J. Chem. Phys.* **1992**, *97*, 2571–2577; b) F. Weigend, R. Ahlrichs, *Phys. Chem. Chem. Phys.* **2005**, *7*, 3297–3305.

[56] a) D. A. Pantazis, X.-Y. Chen, C. R. Landis, F. Neese, *J. Chem. Theory Comput.* **2008**, *4*, 908–919; b) D. A. Pantazis, F. Neese, *J. Chem. Theory Comput.* **2009**, *5*, 2229–2238; c) D. A. Pantazis, F. Neese, *J. Chem. Theory Comput.* **2011**, *7*, 677–684; d) D. A. Pantazis, F. Neese, *Theor. Chem. Acc.* **2012**, *131*, 1292.

[57] R. J. Bouma, J. H. Teuben, W. R. Beukema, R. L. Bansemer, J. C. Huffman, K. G. Caulton, *Inorg. Chem.* **1984**, *23*, 2715–2718.

[58] J. J. H. Edema, W. Stauthamer, F. Van Bolhuis, S. Gambarotta, W. J. J. Smeets, A. L. Spek, *Inorg. Chem.* **1990**, *29*, 1302–1306.

[59] L. I. Belen'kii, V. Z. Shirinyan, G. P. Gromova, A. V. Kolotaev, Y. A. Strelenko, S. N. Tandura, A. N. Shumskii, M. M. Krayushkin, *Chem. Heterocycl. Compd.* **2003**, *39*, 1570–1579.